RESEARCH PAPER

Structural analysis of aluminium-titanium-stainless steel three-layer composites produced by explosive welding

I. Galvão[1,2] · G. H. S. F. L. Carvalho[2,3] · J. Pimenta[4] · T. Abreu[2] · C. Leitão[2] · R. M. Leal[2,5] · R. Mendes[4]

Abstract

The present work aimed to study the morphological, microstructural, and mechanical properties of Al sheet-Ti sheet-SS sheet composites produced by explosion welding. Trimetallic composites with sound structure and very good mechanical behaviour were obtained. The mechanical performance of the produced composites makes them very appropriate for applications requiring increased lightness, corrosion resistance, and mechanical properties at high and low temperature. Regarding the weldability of the material trio, the type of the explosive mixture was found to have a strong influence on the results. Better conditions were achieved by using a mixture with a lower detonation velocity, as high detonation velocities are not appropriate for welding low melting temperature flyers, like aluminium alloys. Although IMC-rich zones were formed at the Al-Ti and Ti-SS interfaces of the composites, these regions were encompassed/accommodated by ductile interfacial waves, which allowed to overcome the brittleness of the IMC regions and to achieve composites with an improved performance. An encompassing literature-based study also allowed to infer that, regardless of the material couples being joined by EXW, the matrix of the intermediate regions formed at the weld interface is always richer in the main element of the welded couple with lower melting temperature.

Keywords Trimetallic composites · Explosion welding · Chemical composition · Mechanical properties · Surface modification · Interface phenomena

1 Introduction

The joining of dissimilar alloys allows the production of metal composites combining properties very difficult to be achieved with a single material. It is not easy to find a conventional material with the same group of properties as

✉ G. H. S. F. L. Carvalho
  gustavo.carvalho@unifi.it

1 UnIRE, ISEL, Polytechnic University of Lisbon, Lisbon, Portugal

2 CEMMPRE, Department of Mechanical Engineering, Univ Coimbra, Coimbra, Portugal

3 Department of Industrial Engineering, University of Florence, Florence, Italy

4 Univ Coimbra, ADAI, LEDAP, Coimbra, Portugal

5 LIDA-ESAD.CR, Polytechnic University of Leiria, Leiria, Portugal

an aluminium (Al)-titanium (Ti)-stainless steel (SS) composite, which combines the low density of Al, the specific strength of Ti and the corrosion resistance and toughness at low temperatures of SS. Although Ti alloys combine corrosion resistance with fairly low density and good mechanical strength, they also present a significantly greater cost than the other two materials, which makes Al-Ti-SS components a much more economical solution than components exclusively composed of Ti, especially for the case of very thick parts [1]. As a result of this, Al-Ti-SS components are extremely attractive to several industries, standing out in industries where the parts experience harsh environments in terms of pressure, corrosion, and temperature, such as aerospace, chemical, shipbuilding, national defence, and marine [2, 3].

Despite the industrial interest of the Al-Ti-SS composites, they cannot be produced by conventional fusion welding due to their differences in physical properties and the susceptibility of forming large quantities of brittle intermetallic compounds (IMCs) when melted together. On the other hand, the solid-state welding techniques have a

strong potential to produce these components. Among the solid-state techniques, the short-cycle processes, like explosion welding (EXW), are especially suitable to join these materials, as they promote a quite short interaction of the materials at high temperature during the welding. These processes, besides minimising the interaction of the materials, which is especially relevant for couples with great tendency for the formation of brittle IMCs, such as Al-Ti [4–6] and steel-Ti [7–9], also lead to the formation of minimal heat affected zones (HAZ). In fact, the joining of the materials is promoted by the coupled effect of high temperature and extreme plastic strain in a quite narrow zone close to the weld interface.

Regarding EXW process, it is especially interesting for surface improvement and modifications because it is capable of modifying a large area of the component very quickly and with narrow heat affected zones. This fact does increase the interest in the process for cladding of corrosion resistant or difficult to weld materials. Moreover, the possibility of performing a three-layer 'sandwich' composite structure in one operation that modifies both surfaces of the component is a very important advantage. The production of Al-Ti-SS composites by EXW has not been fully explored in the literature yet. Even so, Liang et al. [3] studied the microstructure and phase composition of AA1060/TA2/SS30408 composites. The composites were produced using an explosive emulsion sensitised with glass microspheres, whose detonation velocity was 2400 m/s. According to these authors, both the Al/Ti and Ti/SS interfaces were found to be wavy and absent of defects. However, the results from computed tomography allowed to observe significant differences in the 3D morphology of the interfaces. Specifically, the Al/Ti interface was reported to present a morphology looking like 'ripples on the water', while the Ti/SS interface morphology looked more like a 'desert after the wind'. The mechanical behaviour of the composites was not analysed in this research.

Although research on Al-Ti-SS EXW is very scarce, some works have already been conducted on Al-Ti and Ti-SS composites. Regarding the Al-Ti couple, previous works pointed to the formation of vortex zones at the weld interface, in which localised melting occurs and stable and metastable phases are formed [4, 5]. In particular, Pei et al. [6] studied the correlation between the microstructure and phase composition of the composite interface and the fracture behaviour. These authors reported that microcracks are easily induced in the IMC-rich local melting zones of the weld interface in tensile testing. For higher values of deformation, they observed that cracking in these zones caused local delamination of the interface. Mechanical characterisation of Al-Ti composites was also conducted by E et al. [10] and Zhai et al. [11]. Specifically, E et al. [10] studied the behaviour of the composites under dynamic and quasi-static uniaxial tension experiments with the loading direction perpendicular and parallel to the interface. According

to these authors, the composites presented strong anisotropy in yield strength, ductility, and strain rate sensitivity. The strength of the Al/Ti composite was also studied by Zhai et al. [11], who reported an average shear strength of 102 MPa and an average bonding strength of 70 MPa.

Regarding Ti-SS joining, Kahraman et al. [12] conducted one of the pioneer works in this field. These authors characterised the interface morphology and microstructure and tested the bending and tensile-shear behaviours of the composites. The specimens were bent until 180°, and no fracture was observed for all the specimens, while fracture was found to occur outside the interface in tensile-shear testing. More recently, Ti-SS composites were produced by Chen et al. [13], using two different stainless steels, i.e. an austenitic and a duplex steel. The authors reported differences in the interface wave amplitude according to the welded steel, with the austenitic stainless steel-based composites displaying greater values. On the other hand, greater shear strength values were reported to be achieved by the composites produced with duplex stainless steel. These authors also reported that the increase in the dimension of the vortex zones at the weld interface had a detrimental effect on the interfacial strength of the composites. More recently, the interfacial microstructure and the mechanical properties of Ti/AISI 316 welded composites was analysed by Sherpa et al. [1]. Different standoff distances (STD) were tested by these authors and their effect on the properties of the composite interface was analysed. Both the wavelength and the amplitude were found to increase with increments in the STD. For the tested thickness of the plates (3 mm), a STD value of 10 mm provided the best tensile-shear strength both parallelly and perpendicularly to the welding direction.

Considering the research already conducted in Al-Ti and Ti-SS EXW and the industrial interest of Al-Ti-SS composites, which remain almost unexplored in the literature, the development of works in this field is mandatory. The combination of Al, Ti, and SS represents an unusual combination that is able to provide different type of surface modification at just one operation. So, the present research was aimed to study the morphological, microstructural, and mechanical properties of Al-Ti-SS composites produced by EXW. Two different explosive mixtures were used to produce the composites, which were characterised using a large range of techniques, such as scanning electron microscopy (SEM), energy dispersive spectroscopy (EDS), electron backscattering diffraction (EBSD), microhardness, and tensile-shear testing combined with digital image correlation (DIC).

2 Experimental procedure

Al-Ti-SS composites were produced by EXW. The welded materials were the 6082-T6 aluminium alloy, Ti6Al4V titanium alloy, and AISI 304 stainless steel. The AA6082-T6

Table 1 Welding parameters used to produce the composites

Welding conditions	Weld series	
	AF	EE
Flyer alloy	AA6082	AA6082
Intermediate alloy	Ti6Al4V	Ti6Al4V
Baseplate alloy	AISI 304	AISI 304
Explosive mixture	ANFO	EE + EPS
R	3.1	1.3
STD_1	4.5 mm	4.5 mm
STD_2	1.5 mm	1.5 mm

and AISI 304 plates were 3-mm-thick, while the Ti6Al4V plate was 1-mm-thick. The composites were produced in full overlap parallel configuration, with the AA6082-T6 being welded as the flyer plate, the Ti6Al4V as the intermediate plate, and the AISI 304 as the stationary baseplate.

Table 1 shows the welding parameters used to produce the composites. Two weld series (AF and EE) were produced. The AF welds were performed with an ammonium nitrate fuel oil (ANFO) explosive mixture, and the EE welds were produced with an ammonium nitrate-based emulsion explosive (EE) sensitised with expanded polystyrene (EPS) spheres in order to reduce its detonation velocity (V_d) [14]. The explosive ratios (R) of both weld series, i.e. the explosive mixture mass to the flyer plate mass ratio, were different (AF series: $R = 3.1$; EE series: $R = 1.3$). In fact, besides the different densities of the mixtures, the minimum explosive thickness required to detonate varied according to the tested mixture. The STD values, which correspond to the initial distances between the plates, were the same for both weld series. The distance between the flyer and the intermediate plate (STD_1) was 4.5 mm, and the distance between the intermediate and the baseplate (STD_2) was 1.5 mm.

The detonation velocity was measured in all tests according to the procedure adopted by Mendes et al. [15]. The samples for macro and microstructural analysis were removed longitudinally to the welding direction. The samples for the microstructural analysis were prepared according to ASTM E3-11 standard and were observed in a Zeiss Merlin VP Compact scanning electron microscope equipped with EDS. The microstructural analysis was complemented by EBSD, using a FEI Quanta 400FEG SEM equipped with a TSL-EDAX EBSD unit and the OIM analysis software. The mechanical properties of the welds were studied by tensile-shear and microhardness testing. For each welding condition, three tensile-shear specimens with the geometry reported in Carvalho et al. [16–18] were removed longitudinally to the welding direction and tested in a 100 kN universal testing machine Shimadzu AGS-X, using a deformation speed of 1 mm/min. DIC analysis was used during the tests in order to obtain the local strain fields of the specimens using a GOM ARAMIS 5M system. The specimen preparation for the DIC analysis followed the procedure described in Leitão et al. [19]. After the tensile-shear tests, fractography was performed on the fracture surfaces using SEM/EDS. The Vickers microhardness tests were conducted with an HMV-G Shimadzu machine using two different methodologies. The first consisted of performing HV0.2 indentation lines with a distance of 250 μm between indentations along the thickness direction of the longitudinal weld cross-section samples. Based on these results, hardness maps were plotted in order to illustrate the hardness evolution over the longitudinal section. In addition to these indentation lines, local HV0.025 indentations were performed in specific regions of the weld interface.

3 Results and discussion

3.1 Composite joining

Table 2 shows the measured values of detonation/collision point velocity (V_d, V_c), the computed values of impact velocity (V_p), and the welding results. The values of detonation and collision point velocities displayed in the table are the same because the plates were welded in parallel arrangement. As an intermediate plate was used, two values of impact velocity and angle were computed for each weld series, which correspond to the first impact (flyer plate against the intermediate plate) and the second impact (flyer + intermediate set against the baseplate). The impact velocity of the flyer plate on the intermediate plate (V_{pF}) was computed using Gurney's equation for a one-dimensional problem in parallel configuration (Eq. (1)) [20, 21]. However, although this equation is widely accepted in the literature, it has some limitations because it ignores the acceleration of the flyer plate, only representing the terminal velocity [21, 22]. The proximity of the real value to the one calculated with Gurney's equation depends on the effective value of STD.

$$V_{pF} = \sqrt{2E} \left(\frac{3R^2}{R^2 + 5R + 4} \right)^{\frac{1}{2}} \tag{1}$$

$\sqrt{2E}$ is the Gurney characteristic velocity (m.s^{-1}) of the explosive mixture. This parameter was estimated based on

Table 2 Detonation/collision point velocities and welding results

Weld series	V_d, V_c (m.s^{-1})	V_{pF} (m.s^{-1})	V_{pFI} (m.s^{-1})	Welding results
AF	2169	726	466	Consistent
EE	3184	697	444	Consistent

an empirical correlation developed by Cooper [23] for ideal explosives, $\sqrt{2E} = {V_d}/{2.97}$. The limitations of this approach were discussed by Carvalho et al. [24].

The impact velocity of the set composed of the flyer and the intermediate plates on the baseplate (V_{pFI}) was computed using an approximate method considering the perfectly inelastic collision theory and the momentum conservation (Eq. (2)).

$$V_{pFI} = \frac{m_F V_{pF}}{m_F + m_I} \tag{2}$$

m_F and m_I are the masses of the flyer and the intermediate plates (kg), respectively.

From Table 2, it can be observed that, although the explosive mixtures used to produce the AF and EE welds have very different detonation velocities, the impact velocities were fairly similar. This results from the very different densities of the explosive emulsion and ANFO, which promoted a higher explosive ratio for the AF welding. The table also shows that the use of a Ti intermediate plate promoted an important reduction of the impact velocity (about 35%), which allowed to reduce the energy lost in collision [25]. This is well known to favour the welding conditions of metallic couples that easily form IMCs [26], such as Ti and SS. In fact, the tested welding parameters made it possible to produce consistent welded composites, without the separation of the plates after the impact, a usual problem in direct Al-SS welding, for instance [27].

3.2 Composite interface morphology

Micrographs of the longitudinal cross-section of the composites are illustrated in Fig. 1. It can be observed that important differences exist in the morphology of the Al-Ti interface of both weld series. While a flat interface with localised step-like irregularities was formed in the AF welds (Fig. 1a), an interface composed of well-defined waves was formed in the EE welds (Fig. 1b). On the other hand, the figure shows that a wavy morphology was observed at the Ti-SS interface of both weld series. However, the wavelength and amplitude were found to vary according to the explosive mixture used to produce the welds. As shown in Table 3, lower amplitude and wavelength values were measured for the EE welds. Even the step-like irregularities observed at the Al-Ti interface of the AF welds have a higher amplitude and length than the waves formed in the EE welds. These results, which are in good agreement with the results of previous works on Al-SS welding with an Al interlayer [16, 18], point to a very strong effect of the explosive mixture on the wave characteristics. In fact, although the impact velocity is often indicated to be a parameter with a strong influence on the wave parameters [28], the impact velocities registered in AF and EE welding were only slightly different, which corroborates the influence of the explosive base on the wave characteristics. In fact, some authors report the effect of the explosive ratio on the morphology of the waves, in which the amplitude and wavelength are directly proportional to the ratio. In other words, by increasing the ratio, the dimensions of the waves are often reported to increase [29, 30].

Table 4 displays the values of the wave interface factor (WIF) and the impedance mismatch parameter (IMP) calculated to the Al-Ti and Ti-SS interfaces, which are empirical parameters developed by Carvalho et al. [24] and Carvalho et al. [17] that indicate the type of morphology expected for dissimilar metal combinations. The table shows the WIF and IMP calculated and the actual morphologies obtained for the interfaces in the present

Table 3 Wavelength and amplitude of the interfacial waves of the welds

Weld series	Interface	Amplitude (μm)	Wavelength (μm)
AF	Al-Ti[a]	79.6	2142.0
	Ti-SS	119.2 ± 8.9	639.8 ± 11.3
EE	Al-Ti	54.0 ± 7.3	356.3 ± 58.2
	Ti-SS	42.3 ± 7.8	306.0 ± 52.1

[a]No interfacial waves were formed, but step-like irregularities. As the number of measurements was quite smaller than in the other cases, no standard deviation was computed

Fig. 1 Micrographs of the weld longitudinal cross-sections by SEM: **a** AF weld; **b** EE weld
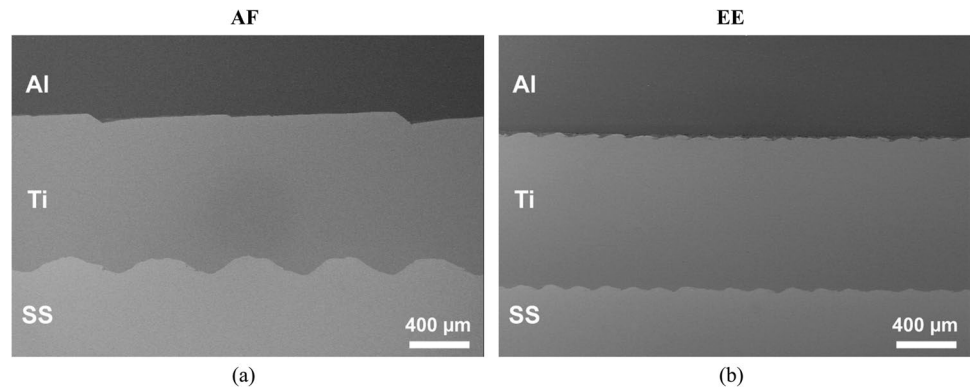

AF

(a)

EE

(b)

Table 4 Interface morphology parameters, predicted morphology/shape, and obtained results

Interface morphology parameters	Al-Ti	Ti-SS
WIF [24]	0.20	0.63
Predicted morphology	Wavy	Wavy
Results	Irregular flat/wavy	Wavy
IMP [17]	0.33	0.41
Predicted morphology	Curled [a]	Curled [a]
Results	Slightly curled	Slightly curled

[a] IMP values corresponding to a shape transition range, for which the actual wave shape may be difficult to define

Table 5 Collision point velocity values for the Al-Ti interface: Cowan's theory; AF weld; EE weld

Cowan's $V_{c,min}$ (m.s^{-1})	V_c (m.s^{-1})—AF weld	V_c (m.s^{-1})—EE weld
3763	2169 (58% $V_{c,min}$)	3184 (85% $V_{c,min}$)

research. The computed WIF values are smaller than the threshold value found by Carvalho et al. [24] to avoid the formation of interfacial waves. In good agreement with this, interfacial waves were formed at the Al-Ti interface for the EE welds, and at the Ti-SS interface for both weld series. Well-defined waves were not formed only at the Al-Ti interface of the AF welds, for which step-like irregularities were observed. This may be associated with the detonation velocity of the AF explosive mixture, which may not have been sufficient to promote the wave formation for this interface. In fact, according to Cowen's theory, who found a transition collision point velocity for the wave formation, the minimum value of collision point velocity required for the formation of interfacial waves is given by Eq. 3 [31].

$$V_{c,min} = \left(R_T \frac{2(H_{flyer} + H_{base})}{\rho_{flyer} + \rho_{base}} \right)^{\frac{1}{2}} \tag{3}$$

R_T is the Reynolds number, ρ is the density (kg.m^{-3}), and H is the hardness (Pa).

Table 5 shows the computed $V_{c,min}$ according to the Cowan's equation and the measured collision point velocities of each weld series (Al-Ti interface). The collision point velocities of both weld series are lower than the minimum velocity required for the formation of interfacial waves. Especially the collision point velocity of the AF welds is well below the Cowen's velocity, which makes it possible to infer that the non-formation of interfacial waves for this weld series was associated with the very low detonation velocity of the explosive mixture (58% $V_{c,min}$). On the other hand, the EE weld presented a value closer to the transition $V_{c,min}$, so some small waves are already present.

Regarding the IMP parameter, Table 4 shows that the values computed to the Al-Ti and Ti-SS interfaces are slightly above the threshold value found by Carvalho et al. [17] to provide the formation of curled waves instead of typical symmetrical waves. In good agreement with this, waves with curled characteristics were formed at the Ti-SS interface of the AF welds (Fig. 2a) and at the Al-Ti (Fig. 2b) and Ti-SS (Fig. 2c) interfaces of the EE welds. Even so, the waves formed at the interface of these welds have less intense curled characteristics than those reported in the literature for other dissimilar interfaces, such as Al-copper [26], Al-carbon steel [18], or Al-niobium [17]. In fact, unlike these material couples, which present higher IMP values, the values computed to the Al-Ti and Ti-SS interfaces correspond to values next to the transition between shapes, for which the formed waves may present hybrid characteristics of typical symmetrical and curled shapes. Moreover, Fig. 2 also shows that, regardless of the weld series, the curling material at each interface is the same, i.e. the SS at the Ti-SS interface

Fig. 2 Micrographs of the weld interface: **a** AF weld, Ti-SS interface; **b** EE weld, Al-Ti interface; **c** EE weld, Ti-SS interface
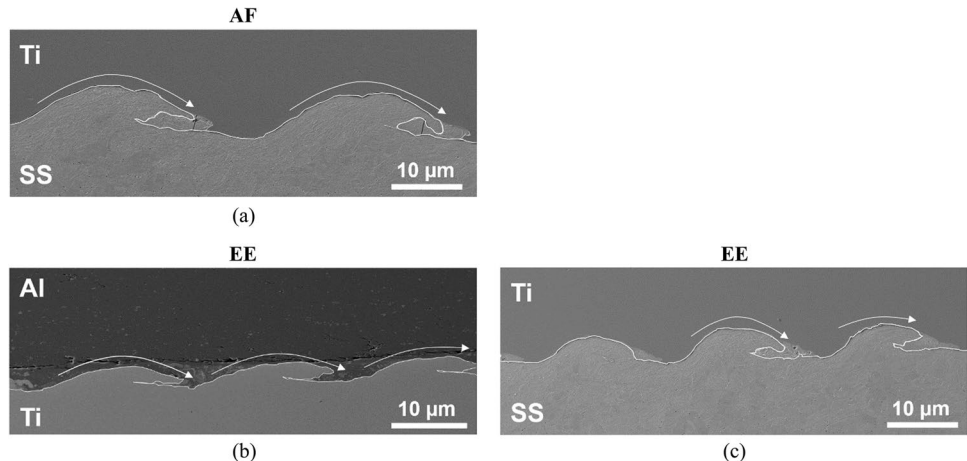
(Fig. 2a, c) and the Ti at the Al-Ti interface (Fig. 2b). According to Carvalho et al. [17], the material curling at the interface is the one with the highest shock impedance, which agrees-well with the present results ($Z_{Al} = 14.5 \times 10^6$ kg.m^{-2}.s^{-1}; $Z_{Ti} = 21.6 \times 10^6$ kg.m^{-2}.s^{-1}; $Z_{SS} = 36.4 \times 10^6$ kg.m^{-2}.s^{-1}). So, because Ti has an intermediate density and impedance between Al and SS, it is the wave-forming material when it interacts with aluminium, while when it interacts with SS, the latter is the wave-forming material. This double behaviour of the Ti alloy in relation to the two other materials proves that the difference in properties between the interacting materials is more important than the alloy's property itself.

3.3 Composite interface microstructure

Figure 3 shows micrographs of the Al-Ti interface of the welds. It can be observed that layers and/or pockets of intermediate material were formed at both the step-like interface of the AF welds (Fig. 3a) and the wavy interface of the EE welds (Fig. 3b). According to Table 6, which displays the EDS results obtained in the regions indicated in the magnified micrographs shown in Fig. 3c, d (R1 to R4), the intermediate regions formed at the Al-Ti interface of both weld series are very rich in Al. The interface micrographs coupled with the elemental maps registered at the Al-Ti interface of the AF welds, which are shown in Fig. 4a, allow to observe that these regions are essentially composed of an Al matrix with Ti–rich IMC particles/fragments dispersed along it. This is in good agreement with the hardness values registered in intermediate regions, which are much higher than the values registered in the neighbour AA6082 alloy (Table 7). In fact, the dispersion of particles with Al-Ti IMC composition along the Al matrix promoted the strengthening of these regions. Even so, it is important to stress that a more uniform material layer was formed inside the curled waves

Fig. 3 Micrographs of the Al-Ti interface: **a** AF weld, lower magnification; **b** EE weld, lower magnification; **c** AF weld, higher magnification; **d** EE weld, higher magnification
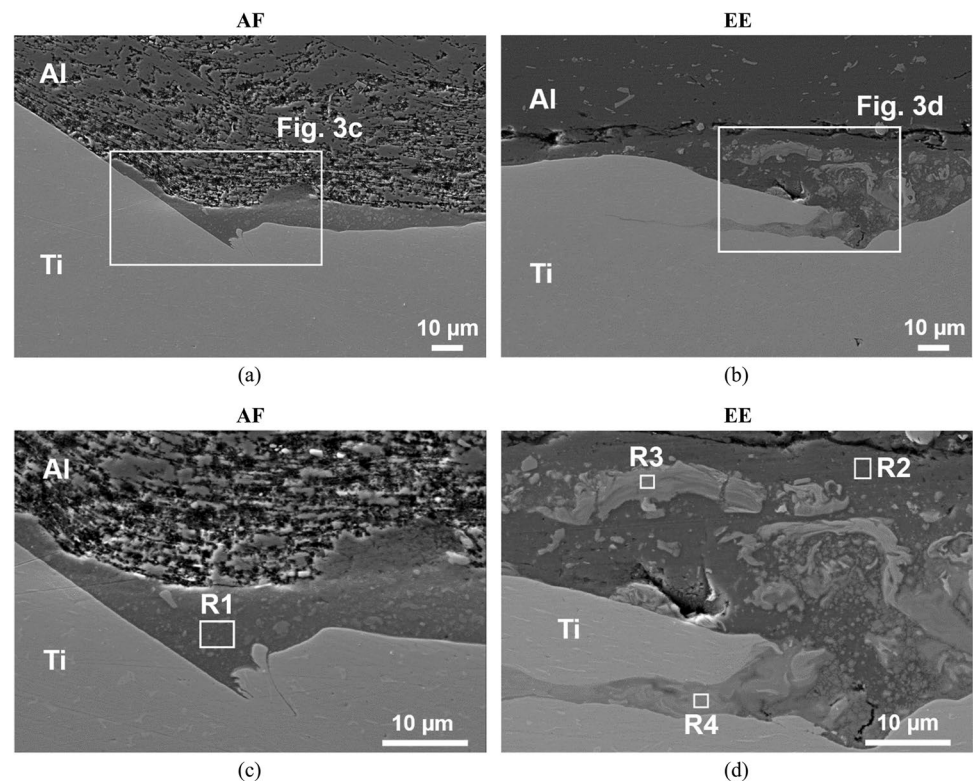
Table 6 Results of the EDS analysis (at.%) conducted in the intermediate material regions

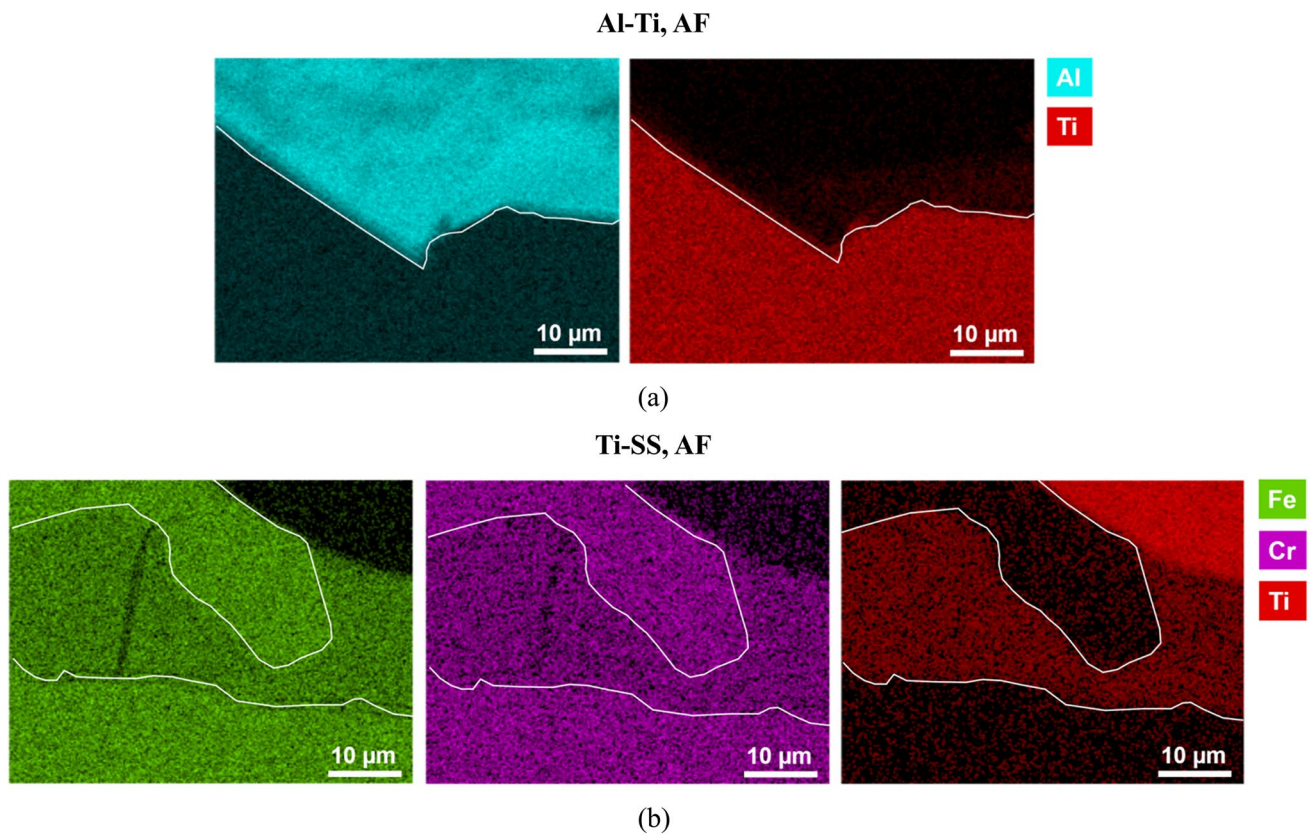| Interface	Weld	Figure	Regions	Al	Ti	Fe	Cr	Ni	Mg	Si	V	Mn
Al-Ti	AF	Figure 3c	R1	94.8	4.4	—	—	—	—	0.7	—	—
	EE	Figure 3d	R2	98.2	0.1	—	—	—	0.7	0.7	—	—
			R3	66.2	32.8	—	—	—	0.5	0.5	—	—
			R4	42.7	54.4	—	—	—	0.3	0.4	2.2	—
Ti-SS	AF	Figure 5c	R5	0.9	9.6	58.9	22.7	7.5	—	0.3	—	—
	EE	Figure 5d	R6	1.5	13.2	57.5	19.0	7.8	—	0.3	0.6	0.1

Al-Ti, AF

(a)

Ti-SS, AF

(b)

Fig. 4 EDS maps of the AF weld: **a** Al-Ti interface; **b** Ti-SS interface. Only the maps regarding the main elements present at each interface are indicated in the figure

Table 7 Hardness values registered at the interface of the welds

Interface	Weld	Weld interface hardness ($HV_{0.025}$)			
		AA6082	Ti6Al4V	AISI 304	Intermediate
Al-Ti	AF	110–115	340–360	——	230–240
	EE	110–115	365	——	130–265
Ti-SS	AF	——	360–370	390–420	670–900
	EE	——	375–395	410–460	600–1200

of the Al-Ti interface of the EE welds. These zones correspond to the vortex regions, where temperature and plastic deformation peaks were reached [32], which resulted in a more uniform mixture of the elements, and consequently, in a richer IMC composition. Despite the richer presence of IMCs inside the curled waves, these zones cannot be considered a focus of brittleness for the welds, as this intermetallic material is entirely surrounded by ductile titanium, which prevents their detrimental effect on the weld mechanical behaviour [17].

Figure 3b shows the formation of a severe discontinuity at the Al-Ti interface of the EE welds. This discontinuity led to the separation of the materials during the preparation of the tensile-shear specimens. This weld was produced with a high detonation velocity mixture, which has already been reported to have a very detrimental effect on dissimilar welding, especially when aluminium alloys are welded as the flyer plate. In fact, Carvalho et al. [33] detected this phenomenon in Al-Cu explosive welding, showing that interfacial melting occurs more easily when the aluminium alloy is welded as the flyer plate. They showed that, when aluminium is the flyer, lower values of energy lost by the collision and lower collision point velocities are needed to cause interfacial melting, which makes the weld more susceptible to separate upon impact.

Micrographs of the Ti-SS interface of the welds are illustrated in Fig. 5. As often observed for waves with a curled shape, the intermediate material was formed inside each wave, extending some micrometres outside it, for both weld series (Fig. 5a, b). From the magnified micrographs shown in Fig. 5c, d, it can be observed that the intermediate material formed at the Ti-SS interface has a more uniform morphology than the material formed at the Al-Ti interface. In fact, the elemental maps obtained at the Ti-SS interface of the AF weld, which are displayed in Fig. 4b, corroborate the more uniform morphology of this region, showing a uniform

Fig. 5 Micrographs of the Ti-SS interface: **a** AF weld, lower magnification; **b** EE weld, lower magnification; **c** AF weld, higher magnification; **d** EE weld, higher magnification
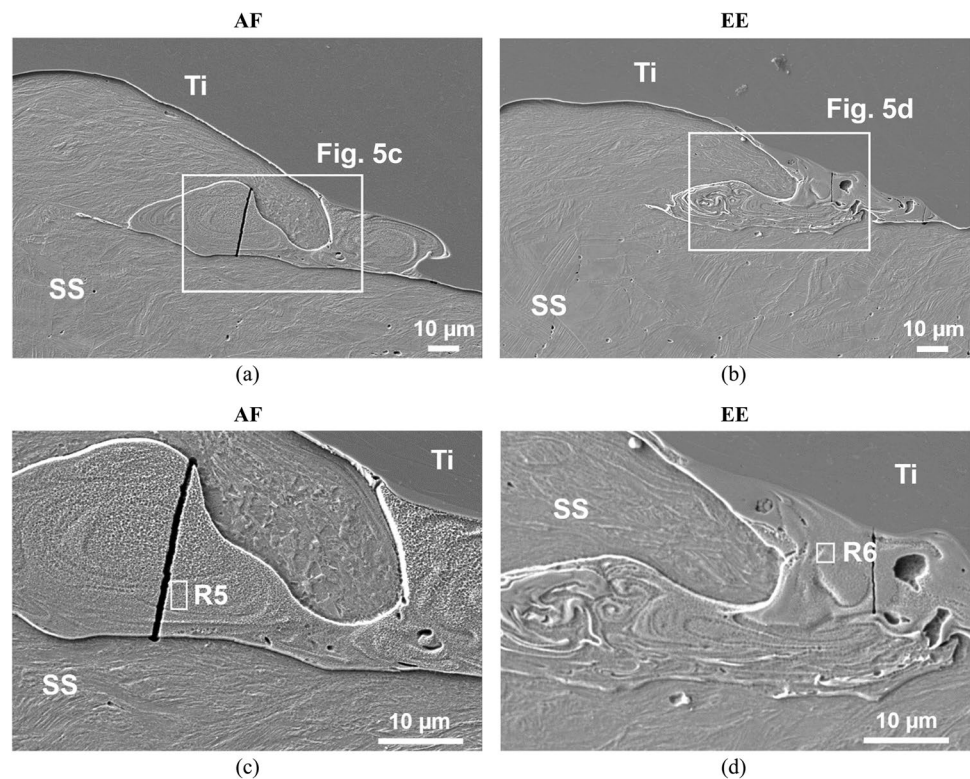
distribution of the three main elements composing the intermediate material, i.e. Fe, Cr, and Ti. However, according to Table 6, which displays the EDS results obtained in the regions indicated in Fig. 5c, d, the atomic composition in Fe is much higher than the composition in Ti and the remaining alloy elements of the Ti6Al4V alloy.

Besides having a mixed chemical composition, the intermediate regions formed at the Ti-SS interface of both weld series also present very high hardness values (Table 7), which points to the formation of hard and brittle IMCs during welding. In good agreement with this, some microcracks can be observed all over the Ti-SS intermediate zones, whose propagation is blocked by the ductile Ti6Al4V and stainless steel layers existing around these regions. The morphology and the hardness values of the Al-Ti and Ti-SS intermediate regions point to important differences in their intermetallic composition. Effectively, the Ti-SS intermediate regions present a much more uniform morphology and much higher hardness values, which indicates a more significant presence of IMCs.

Analysing the interface more deeply through EBSD, the inverse pole figures (IPF) in Fig. 6 indicate that there is deformation of the grains adjacent to the interface in both aluminium (Al-Ti interface, Fig. 6a) and steel (Ti-SS interface, Fig. 6b). The formation of grains with smaller dimension and equiaxed shape also suggest the occurrence of recrystallization at the weld interface as a result of the coupled effect of heating and extreme plastic strain [34].

Furthermore, as shown in Fig. 6c, IMCs were identified at both interfaces. However, it should be noted that the phase analysis conducted by EBSD was used only to make the presence of IMCs at the weld interface evident. In fact, this analysis was extremely localised, and therefore, other phases beyond those indicated by the Kikuchi patterns may exist.

3.4 Composites mechanical behaviour

Hardness maps obtained over the longitudinal cross-section of the welds are illustrated in Fig. 7. The hardness maps encompass the entire area of the weld cross-section, excluding the interface zone, whose values are displayed in Table 7. From the maps, it can be observed that the welding process did not promote significant differences in the hardness of the AA6082, as the values after welding are similar to the base material hardness (114 $HV_{0.2}$). As shown in Table 7, the hardness of the aluminium alloy is quite similar to the base material hardness even in the zones closest to the weld interface. In fact, as AA6082 is a heat-treatable alloy, its main hardening mechanism is not plastic deformation, but precipitation. As the heating is instantaneous and highly concentrated in explosive welding, the thermomechanical affected zone is very narrow zone and the thermal cycle experienced by the AA6082 was not enough for changing the structure and density of the second-phase particles. Hence, the small effect on the alloy hardness.
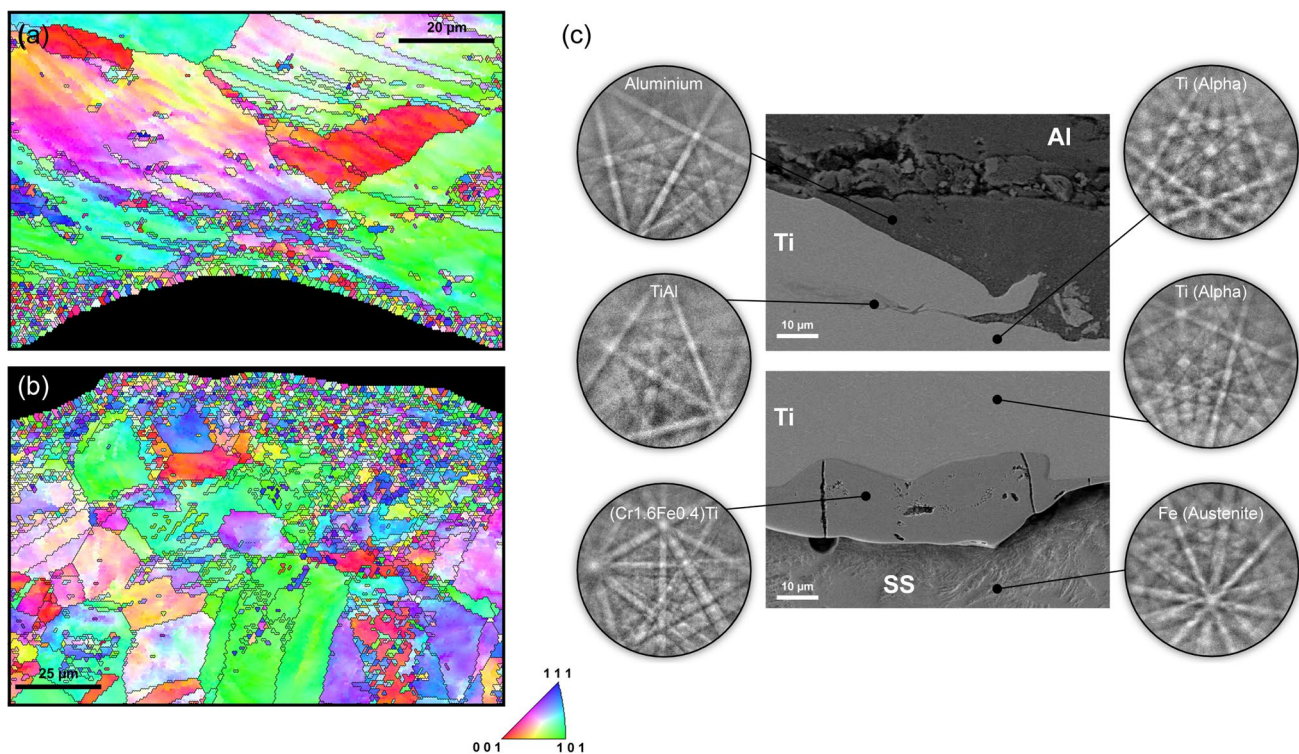
Fig. 6 IPF of the aluminium (**a**) and stainless (**b**) steel interfaces, and SEM images with the Kikuchi patterns identifying the phases (**c**) for the EE weld series

Figure 7 also shows that the welding process had a minor effect on the hardness of the Ti-6Al-4V alloy. The hardness values registered over the intermediate plate tend to be similar to the base material hardness (350 HV). On the other hand, a strong hardening was observed all over the AISI 304 plate, reaching values that are about twice the base material hardness (188 HV0.2). Moreover, an extremely hardened region was formed near the weld interface, where occurred the most intense plastic strain. Although the hardness values reached in this zone are similar in both weld series, the dimensions of the extremely hardened regions are different, being larger in the AF weld, which may be associated with the higher explosive ratio and impact velocity associated with this joint. These results indicate that these aspects had a stronger influence on the extension of the extremely hardened region than on the hardness peak values achieved at the weld interface (Table 7).

The energetic material (AF and EE) properties interact with the material to be welded. Although the detonation/collision point velocity (V_d or V_c) has a direct relationship with the impact velocity (V_p), and, consequently, with the kinetic energy transferred to the welding, other factors must be considered. As Eq. (1) shows, both V_d and the explosive ratio (R) affect the impact velocity. However, the impact velocity value alone may not be enough to indicate whether a weld will be consistent or not. This occurs because a high value of V_c with a low ratio can result in the same impact velocity as a low V_c with a high ratio (Eq. (1)). The present work shows that similar values of V_p resulted in very different results because of the differences in V_d and explosive ratio combinations. It is important that the energetic mixture chosen is capable of being used with reasonable ratio values, avoiding the combination of very high V_c with very low explosive ratio, which can more easily result in failed welds.

Table 8 and Fig. 8 display the tensile-shear testing results of the welds for the AF weld series. Regarding the EE weld series, the joints were not tested because the specimens fractured during machining due to a material discontinuity that formed at the Al-Ti interface, which severely affected the weld mechanical behaviour. Table 8 shows the range of maximum load values and the fracture location for the AF weld series and for previous works on Al-SS joining, in which the same specimen geometry was used. In turn, Fig. 8 illustrates the Von Mises' strain distribution map at maximum load (Fig. 8a) and the specimen macrograph after fracture (Fig. 8b). From Table 8, it can be observed that the maximum load values registered for the AF welds ranged between 9.5 and 10.1 kN, which points to a very regular behaviour for all the tested specimens. As illustrated in Fig. 8, although localised strain was found in the aluminium and stainless steel regions of the specimens (Fig. 8a), they failed at the Ti-SS interface (Fig. 8b), where no strain was observed.

Fig. 7 Hardness maps obtained along the longitudinal cross-section of the welds: **a** AF weld; **b** EE weld
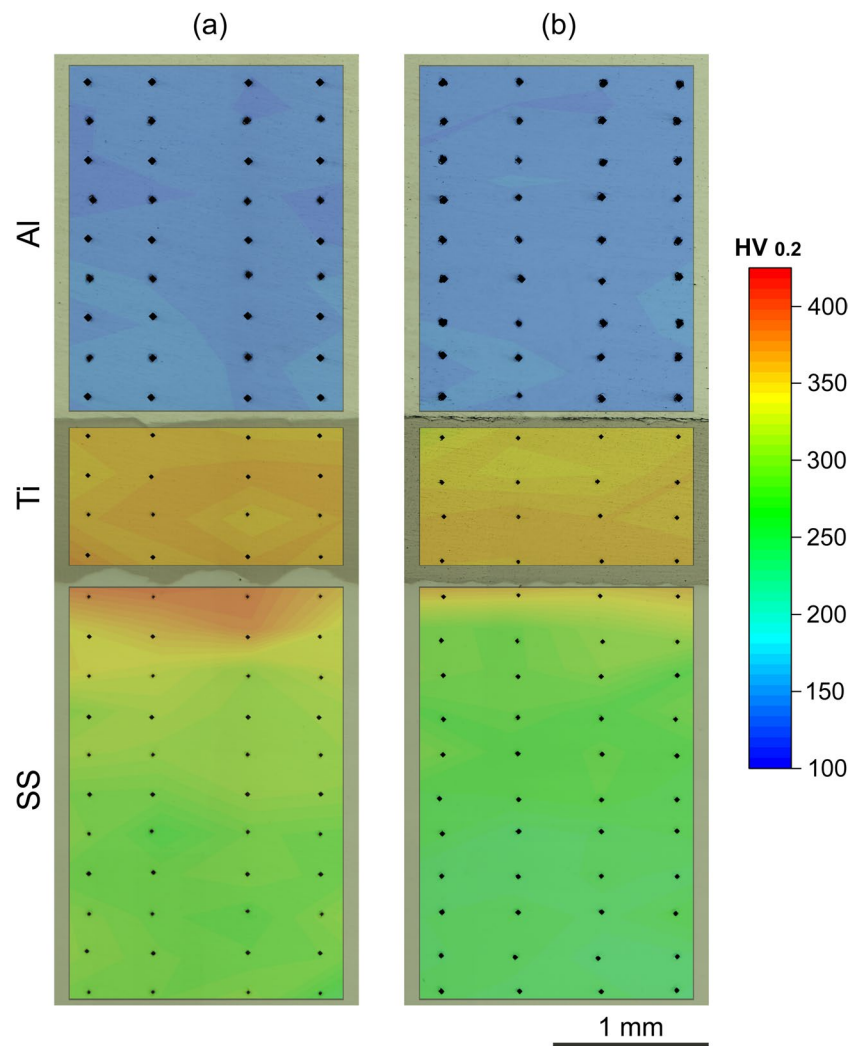
These results suggest that a brittle fracture occurred in this zone. Effectively, the fractographic study (Fig. 9), shows that cleavage occurred at the Ti-SS interface. In good agreement with this, both the lower (Fig. 9a) and higher magnification (Fig. 9b) micrographs of the fracture surface show several cracks propagating through the brittle structures.

Table 8 Tensile-shear testing results obtained in current and previous works on Al-SS explosive welding

Works	Welds	Maximum load (kN)	Failure zone
Current	Al-Ti-SS (AF)	9.5–10.1	Ti-SS weld interface
	Al-Ti-SS (EE)	NST	———
[18]	Al-SS	NST	———
	Al-Al-SS	NST–6.0	Interlayer
[16]	Al-Al-SS	4.5–5.0	Interlayer
[17]	Al-CS-SS	11.4–11.5	Outside the weld
	Al-Nb-SS	8.8–11.0	Outside the weld

NST not enough strength to be tested

Table 9 displays the results of the EDS analyses performed in the regions indicated in Fig. 9, which shows that a mixed chemical composition was detected in all the tested regions of the fracture surfaces. The chemical compositions match-well the composition of the intermediate regions formed at the Ti-SS interface, which confirms that the formation of IMCs-rich regions at the weld interface affected the mechanical behaviour of the welds. However, as curled waves were formed at the Ti-SS interface, the brittleness of the IMC-rich material was to some extent accommodated by the ductile waves [18], allowing the plastic deformation of the aluminium and stainless steel regions, instead of the premature failure of the specimens. In order to further improve the mechanical properties of the joints and avoid fracture at the interface, it is necessary to find welding parameters capable of promoting the formation of waves with morphologies that surround the brittle intermetallic compounds. Some examples of these morphologies are presented in previous works for other dissimilar metallic combinations [17, 18].

Fig. 8 AF weld specimen during tensile-shear testing: **a** maximum load instant (DIC strain map); **b** after fracture
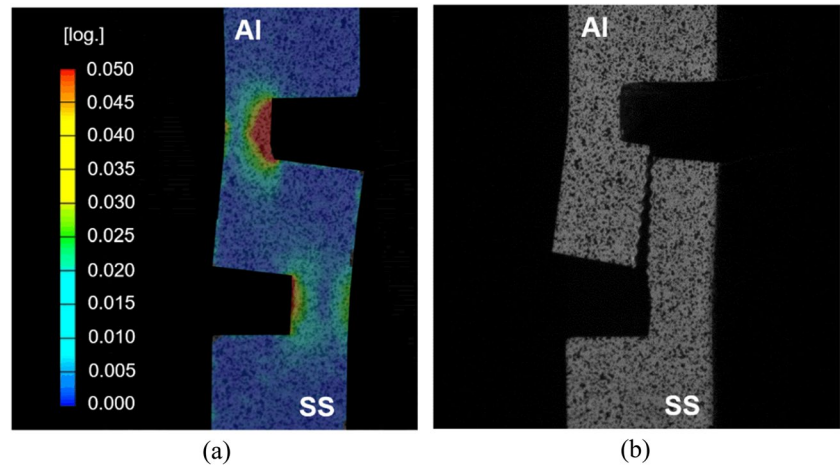

(a)

(b)

Fig. 9 SEM micrographs of the fracture surface of the AF weld series: **a** lower magnification; **b** higher magnification
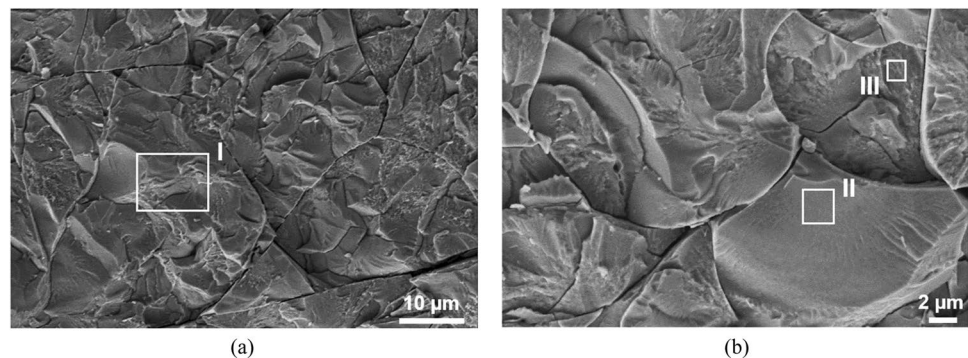

(a)

(b)

Table 9 Results of the EDS analysis (at.%) conducted in the fracture surface of the AF welds

Regions	Al	Ti	Fe	Cr	Ni
I	2.8	21.5	52.9	14.5	8.3
II	3.5	23.6	50.2	16.3	6.5
III	5.5	41.6	38.7	8.8	5.4

Table 8 shows that, among the bimetallic (Al-SS) and trimetallic (Al-intermediate material-SS) composites, the best mechanical behaviour was achieved for the Al-CS-SS composites, i.e. when a CS intermediate plate was used. In fact, these joints presented the highest values of maximum load and failed outside the weld region. On the other hand, Al-SS welding did not result in composites with enough strength to be tested, being the worst scenario by far (similar to the Al-Ti-SS EE weld series using high detonation velocity). Comparing the results obtained in this research with the remaining displayed in the table, it can be concluded that welding Al and SS with a Ti intermediate plate allows the achievement of composites with good mechanical properties, when welded with lower detonation velocity (as in sample AF). In fact, the maximum load values were only slightly lower than those achieved using a CS or a Nb intermediate plate. Furthermore, the titanium has important advantages when it is compared with these materials, i.e. it is lighter, presents improved corrosion resistance, better mechanical properties at high and low temperature when compared to the CS and it is more economic than Nb.

3.5 Discussion on interface chemical composition

The EDS results showed that the intermediate regions of the AF and EE welds have a mixed chemical composition. Additionally, it was observed that these zones have not a balanced composition between the chemical elements composing the adjoining materials at each interface. Actually, the Al/Ti intermediate regions tend to be much richer in Al, while the Ti/SS regions tend to be much richer in Fe. Even so, as deeply discussed by Greenberg et al. [35] and Bataev et al. [36], these zones are highly heterogeneous, and therefore, some zones of both the Al/Ti and Ti/Fe regions may be locally richer in Ti. These zones are often observed to correspond to fragments of Ti or even Ti–rich IMCs dispersed over the Al-rich or Fe-rich matrix.

In order to better understand the weld intermediate regions, which are often observed in dissimilar joining by

Table 10 Literature-based approach to the chemical composition of the intermediate regions formed at the weld interface for widely explored welded couples

Welded alloys	LMTE	Number of EDS analyses	Analysis richer in LMTE (%)	Works
Al/Fe	Al	23	95.7	[16, 18, 27, 37–39]
Al/Ti	Al	27	85.2	[4–6]
Al/Ni	Al	14	78.6	[40, 41]
Al/Cu	Al	35	91.4	[24, 28, 33, 42–46]
Fe/Ti	Fe	20	100.0	[2, 7–9, 47–50]
Cu/Ti	Cu	20	85.0	[51–56]
Cu/Fe	Cu	11	90.9	[47, 52, 57–61]

EXW regardless of the higher or lower mutual solubility of the elements composing the welded plates, a deep literature survey on the chemical composition of these regions was made. Part of the results of this analysis is displayed in Table 10, which addresses the most explored alloy couples in the literature. The table indicates the lower melting temperature element (LMTE) among the main elements of each alloy couple (for example, Fe in carbon and stainless steels, Ti in titanium alloys, or Cu in copper alloys), the number of EDS analyses considered and the fraction of analysis richer in the element with lower melting temperature. The number of EDS analyses corresponds to the analyses that were considered in the literature-based study, encompassing analyses belonging to different works. It should be noted that the EDS analysis (% at.) considered in the study were conducted in the matrix region of the intermediate zones, and therefore, analysis conducted in particles or fragments exclusively composed of a single element were discarded (all the EDS analysis with a composition greater than 90% at. in a specific chemical element were not considered). As a significant number of analyses were considered for each alloy couple, the fraction of analyses richer in the LMTE of the intermediate region is also displayed in the table. From the table, it can be observed that, regardless of the welded couple, the matrix of the intermediate regions tends be richer in the main element of the welded couple with lower melting temperature. For the material couple with the lowest fraction, it can be observed that about 80% of the EDS analysis spots are richer in the LMTE. Although EDS analysis has several limitations in which concerns to obtain accurate chemical compositions for small analysing areas and the analysis conditions differ among the different works considered in this study, a clear trend on the chemical composition of these zones is observed.

Unlike the alloy couples displayed in Table 10, there are some couples for which the literature data on the chemical

composition of the intermediate regions is much scarcer and only some analysis can be found for each couple. However, although a statistical approach is not suitable to be followed for these couples, a clear trend can also be observed. As displayed in Table 11, the material with the lower melting temperature is dominant in the intermediate regions for most of the alloy couples. This is valid regardless of the magnitude of the difference between the melting temperature of the main elements of the welded alloys.

The formation of intermediate regions in EXW results from the high temperatures and plastic deformation occurring at the weld interface. Usually, these regions are formed in vortex zones, in which the highest peaks in temperature and plastic deformation are reached [32]. According to Greenberg et al. [35], true solutions are formed in local melting zones of the intermediate regions when the alloy elements have mutual solubility, while colloidal solid solutions are formed for immiscible elements. In turn, Bataev et al. [36] reported that depending on the chemical composition of the vortexes they may consist of stable phases predicted by equilibrium phase diagrams, metastable crystalline phases, metastable quasicrystalline phases, metastable glassy phases, or even a mixture of several stable and metastable phases. From the present results, it is observed that regardless of the alloys couple being welded or the location of the alloys as the flyer or baseplate, the LMTE is dominant in the chemical composition of the hybrid matrix of the intermediate region. However, heterogeneity may be observed over these regions because of the very high heating and cooling rates in EXW [36], which explains the formation of local volumes richer in the HMTE. As a result of this, there are several reports in the literature of the formation of IMCs richer in the HMTE, such as Cu_6Sn_5, Ti_3Al, and $CuTi_2$ in the Sn/Cu [67], Al/Ti [6], and Cu/Ti [53] interfaces, respectively. Even so, important information is given to future works devoted to study the phase formation phenomenon in EXW by realising the dominance of the LMTE in the chemical composition of the

Table 11 Literature-based approach to the chemical composition of the intermediate regions formed at the weld interface for less explored welded couples

Welded alloys	LMTE	Intermediate zone's dominant element	Works
Al/Nb	Al	Al	[62]
Fe/Nb	Fe	Nb	[63]
Fe/Zr	Fe	Fe	[64]
Fe/W	Fe	Fe	[65]
Ag/Fe	Ag	Ag	[35, 66]
Cu/Zr	Cu	Cu	[36]
Cu/Ta	Cu	Cu	[59]
Sn/Cu	Sn	Sn	[67]
Ni/Zr	Ni	Ni	[36]

intermediate zones. Moreover, this is also a good input to the selection of the most suitable interlayer to facilitate the welding of a specific couple of alloys, as the composition of the intermediate zones may have a strong influence on the weld mechanical behaviour.

4 Conclusions

The present research was aimed to study the morphological, microstructural and mechanical properties of Al-Ti-SS composites produced by EXW. The following conclusions can be drawn:

- Al-Ti-SS trimetallic composites with sound structure and very good mechanical behaviour can be obtained by EXW. The mechanical performance of these composites is quite similar to other trimetallic composites with excellent performance, like Al-CS-SS and Al-Nb-SS. However, the Ti-based composites stand out for their increased lightness, improved corrosion resistance, and better mechanical properties at high and low temperature (comparing to Al-CS-SS) and lower cost (comparing to Al-Nb-SS).
- The use of explosive mixtures with a lower detonation velocity gives rise to better welding conditions than when an explosive mixture with a higher detonation velocity is used. Although the intermediate and bottom plates of these composites are high-melting temperature materials, the top aluminium plate limits the range of detonation speed that can be used to obtain sound welded composites.
- IMC-rich zones are formed at the Al-Ti and Ti-SS interfaces of the Al-Ti-SS trimetallic composites. The intermetallic content and brittleness of the Ti-SS IMC-rich zones is greater than that of the Al-Ti interfaces. Despite the brittle nature of the composite interfaces, the formation of interfacial waves, which are ductile and encompass/accommodate the brittle IMC-rich regions, allows a very good mechanical performance of the composites.
- Regardless of the material couples being joined by EXW, the matrix of the intermediate regions formed at the weld interface is richer in the main element of the welded couple with lower melting temperature.

Declarations

References

1. Sherpa BB, Kuroda M, Ikeda T et al (2023) Investigation of interfacial microstructure and mechanical characteristics of Ti/SS316 clads fabricated by explosive welding process. Int J Adv Manuf Technol 128:1403–1418. https://doi.org/10.1007/s00170-023-12010-y
2. Xu J, Yang M, Chen D et al (2021) Providing a new perspective for obtaining high-quality metal coatings: fabrication and properties studies of TA2 foil on Q235 steel by explosive welding. Arch Civ Mech Eng 21:1–11. https://doi.org/10.1007/s43452-021-00271-x
3. Liang H, Luo N, Chen Y et al (2022) Interface microstructure and phase constitution of AA1060/TA2/SS30408 trimetallic composites fabricated by explosive welding. J Market Res 18:564–576. https://doi.org/10.1016/j.jmrt.2022.02.109
4. Lazurenko DV, Bataev IA, Mali VI et al (2016) Explosively welded multilayer Ti-Al composites: structure and transformation during heat treatment. Mater Des 102:122–130. https://doi.org/10.1016/j.matdes.2016.04.037
5. Fronczek DM, Wojewoda-Budka J, Chulist R et al (2016) Structural properties of Ti/Al clads manufactured by explosive welding and annealing. Mater Des 91:80–89. https://doi.org/10.1016/j.matdes.2015.11.087
6. Pei Y, Huang T, Chen F et al (2020) Microstructure and fracture mechanism of Ti/Al layered composite fabricated by explosive welding. Vacuum 181:109596. https://doi.org/10.1016/j.vacuum.2020.109596
7. Wang T, Zhang F, Li X et al (2018) Interfacial evolution of explosively welded titanium/steel joint under subsequent EBW process. J Mater Process Technol 261:24–30. https://doi.org/10.1016/j.jmatprotec.2018.05.031
8. Lazurenko DV, Bataev IA, Mali VI et al (2018) Structural transformations occurring upon explosive welding of alloy steel and high-strength titanium. Phys Met Metall 119:469–476. https://doi.org/10.1134/S0031918X18050095
9. Chu Q, Tong X, Xu S et al (2020) Interfacial investigation of explosion-welded titanium/steel bimetallic plates. J Mater Eng Perform 29:78–86. https://doi.org/10.1007/s11665-019-04535-9
10. Jc E, Huang JY, Bie BX et al (2016) Deformation and fracture of explosion-welded Ti/Al plates: a synchrotron-based study. Mater Sci Eng, A 674:308–317. https://doi.org/10.1016/j.msea.2016.07.125
11. Zhai W, Ye C, Deng G et al (2023) Microstructure and mechanical properties investigations of pure titanium-aluminum alloy

composite fabricated by explosive welding. J Mater Eng Perform. https://doi.org/10.1007/s11665-023-08613-x

12. Kahraman N, Gülenç B, Findik F (2005) Joining of titanium/stainless steel by explosive welding and effect on interface. J Mater Process Technol 169:127–133. https://doi.org/10.1016/j.jmatprotec.2005.06.045

13. Xiang C, Inao D, Tanaka S et al (2021) Comparison of explosive welding of pure titanium/SUS 304 austenitic stainless steel and pure titanium/SUS 821L1 duplex stainless steel. Trans Nonferrous Metals Soc China (English Edition) 31:2687–2702. https://doi.org/10.1016/S1003-6326(21)65685-6

14. Pimenta J, Quaresma J, Ribeiro J, Mendes R (2023) Detonation characterization of low-density emulsion explosives. Propellants, Explos, Pyrotech 48:1–9. https://doi.org/10.1002/prep.202300046

15. Mendes R, Ribeiro J, Plaksin I, et al (2014) Differences between the detonation behavior of emulsion explosives sensitized with glass or with polymeric micro-balloons. J Phys Conf Ser 500. https://doi.org/10.1088/1742-6596/500/5/052030

16. Carvalho GHSFL, Galvão I, Mendes R et al (2020) Aluminum-to-steel cladding by explosive welding. Metals (Basel) 10:1–18. https://doi.org/10.3390/met10081062

17. Carvalho GHSFL, Galvão I, Mendes R et al (2020) Explosive welding of aluminium to stainless steel using carbon steel and niobium interlayers. J Mater Process Technol 283:116707. https://doi.org/10.1016/j.jmatprotec.2020.116707

18. Carvalho GHSFL, Galvão I, Mendes R, et al (2019) Microstructure and mechanical behaviour of aluminium-carbon steel and aluminium-stainless steel clads produced with an aluminium interlayer. Mater Charact 155. https://doi.org/10.1016/j.matchar.2019.109819

19. Leitão C, Galvão I, Leal RM, Rodrigues DM (2012) Determination of local constitutive properties of aluminium friction stir welds using digital image correlation. Mater Des 33. https://doi.org/10.1016/j.matdes.2011.07.009

20. Kennedy JE (1970) Gurney energy of explosives: estimation of the velocity and impulse imparted to driven metal. Albuquerque, NM, and Livermore, CA (United States)

21. El-Sobky H (1983) Mechanics of explosive welding. In: Blazynski TZ (ed) Explosive welding, forming and compaction. Applied Science Publishers, Dordrecht, pp 189–217

22. Patterson RA (1993) Fundamentals of explosion welding. ASM handbook—volume 6: welding, brazing and soldering. ASM International, Materials Park, OH, USA, pp 160–164

23. Cooper PW (1996) Explosive engineering. Wiley-VCH, New York, NY, USA

24. Carvalho GHSFL, Mendes R, Leal RM et al (2017) Effect of the flyer material on the interface phenomena in aluminium and copper explosive welds. Mater Des 122:172–183. https://doi.org/10.1016/j.matdes.2017.02.087

25. Hokamoto K, Izuma T, Fujita M (1993) New explosive welding technique to weld aluminum alloy and stainless steel plates using a stainless steel intermediate plate. Metall Trans A 24:2289–2297. https://doi.org/10.1007/BF02648602

26. Carvalho GHSFL, Galvão I, Mendes R, et al (2018) Influence of base material properties on copper and aluminium–copper explosive welds. Sci Technol Weld Join 23. https://doi.org/10.1080/13621718.2017.1417783

27. Carvalho GHSFL, Galvão I, Mendes R, et al (2018) Explosive welding of aluminium to stainless steel. J Mater Process Technol 262. https://doi.org/10.1016/j.jmatprotec.2018.06.042

28. Athar MMH, Tolaminejad B (2015) Weldability window and the effect of interface morphology on the properties of Al/Cu/Al laminated composites fabricated by explosive welding. Mater Des 86:516–525. https://doi.org/10.1016/j.matdes.2015.07.114

29. Gulenc B (2008) Investigation of interface properties and weldability of aluminum and copper plates by explosive welding

30. Fang Z, Shi C, Shi H, Sun Z (2019) Influence of explosive ratio on morphological and structural properties of Ti/Al clads. Metals (Basel) 9. https://doi.org/10.3390/met9020119

31. Cowan GR, Bergmann OR, Holtzman AH (1971) Mechanism of bond zone wave formation in explosion-clad metals. Metall Mater Trans B 2:3145–3155. https://doi.org/10.1007/BF02814967

32. Bataev IA, Bataev AA, Mali VI et al (2014) Structural changes of surface layers of steel plates in the process of explosive welding. Met Sci Heat Treat 55:509–513. https://doi.org/10.1007/s11041-014-9663-7

33. Carvalho GHSFL, Galvão I, Mendes R et al (2019) Weldability of aluminium-copper in explosive welding. Int J Adv Manuf Technol 103:3211–3221. https://doi.org/10.1007/s00170-019-03841-9

34. Paul H, Lityńska-Dobrzyńska L, Prażmowski M (2013) Microstructure and phase constitution near the interface of explosively welded aluminum/copper plates. Metall Mater Trans A Phys Metall Mater Sci 44:3836–3851. https://doi.org/10.1007/s11661-013-1703-1

35. Greenberg BA, Ivanov MA, Rybin VV et al (1970) The problem of intermixing of metals possessing no mutual solubility upon explosion welding (Cu–Ta, Fe–Ag, Al–Ta). Mater Charact 75:51–62. https://doi.org/10.1016/j.matchar.2012.10.011

36. Bataev IA, Lazurenko DV, Tanaka S et al (2017) High cooling rates and metastable phases at the interfaces of explosively welded materials. Acta Mater 135:277–289. https://doi.org/10.1016/j.actamat.2017.06.038

37. Chu Q, Xia T, Zhao P et al (2022) Interfacial investigation of explosion-welded Al/steel plate: the microstructure, mechanical properties and residual stresses. Mater Sci Eng, A 833:142525. https://doi.org/10.1016/j.msea.2021.142525

38. Shmorgun VG, Slautin OV, Kulevich VP (2019) Features of diffusion interaction in steel-aluminum composite after explosive welding and aluminizing by melt immersion. Metallurgist 63:766–774. https://doi.org/10.1007/s11015-019-00887-8

39. Carvalho GHSFL, Galvão I, Mendes R et al (2018) Formation of intermetallic structures at the interface of steel-to-aluminium explosive welds. Mater Charact 142:432–442. https://doi.org/10.1016/j.matchar.2018.06.005

40. Bataev IA, Ogneva TS, Bataev AA et al (2015) Explosively welded multilayer Ni-Al composites. Mater Des 88:1082–1087. https://doi.org/10.1016/j.matdes.2015.09.103

41. Kwiecien I, Bobrowski P, Janusz-Skuza M et al (2020) Microstructure of the interface zone after explosive welding and further annealing of A1050/Ni201 clads using various joining conditions. J Mater Sci 55:9163–9172. https://doi.org/10.1007/s10853-019-04317-7

42. Shiran MKG, Khalaj G, Pouraliakbar H et al (2018) Multilayer Cu/Al/Cu explosive welded joints: Characterizing heat treatment effect on the interface microstructure and mechanical properties. J Manuf Process 35:657–663. https://doi.org/10.1016/j.jmapro.2018.09.014

43. Hoseini-Athar MM, Tolaminejad B (2016) Interface morphology and mechanical properties of Al-Cu-Al laminated composites fabricated by explosive welding and subsequent rolling process. Met Mater Int 22:670–680. https://doi.org/10.1007/s12540-016-5687-4

44. Loureiro A, Mendes R, Ribeiro JB et al (2016) Effect of explosive mixture on quality of explosive welds of copper to aluminium. Mater Des 95:256–267. https://doi.org/10.1016/j.matdes.2016.01.116

45. Carvalho GHSFL, Galvão I, Mendes R et al (2018) Influence of base material properties on copper and aluminium–copper explosive welds. Sci Technol Weld Joining 23:501–507. https://doi.org/10.1080/13621718.2017.1417783

46. Carvalho GHSFL, Galvão I, Mendes R et al (2019) Friction stir welding and explosive welding of aluminum/copper: process analysis. Mater Manuf Processes 34:1243–1250. https://doi.org/10.1080/10426914.2019.1644452

47. Li X, Bi Z, Wang Q et al (2023) Influence of copper foil interlayer on microstructure and bonding properties of titanium-steel explosive welded composite plate. Mater Today Commun 34:105143. https://doi.org/10.1016/j.mtcomm.2022.105143

48. Yang M, Ma HH, Shen ZW (2019) Study on explosive welding of Ta2 titanium to Q235 steel using colloid water as a covering for explosives. J Market Res 8:5572–5580. https://doi.org/10.1016/j.jmrt.2019.09.025

49. Bi Z, Li X, Yang K et al (2023) Experimental and numerical studies of titanium foil/steel explosively welded clad plate. Def Technol 25:192–202. https://doi.org/10.1016/j.dt.2022.05.001

50. Arisova VN, Gurevich LM, Trudov AF et al (2019) Structure formation in the zones of joints obtained by explosion welding with subsequent rolling of a five-layer titanium-steel composite. Metallurgist 63:96–104. https://doi.org/10.1007/s11015-019-00798-8

51. Mahmood Y, Chen PW, Bataev IA, Gao X (2021) Experimental and numerical investigations of interface properties of Ti6Al4V/CP-Ti/copper composite plate prepared by explosive welding. Def Technol 17:1592–1601. https://doi.org/10.1016/j.dt.2020.09.003

52. Chu Q, Cao Q, Zhang M et al (2022) Microstructure and mechanical properties investigation of explosively welded titanium/copper/steel trimetallic plate. Mater Charact 192:112250. https://doi.org/10.1016/j.matchar.2022.112250

53. Paul H, Chulist R, Miszczyk M, et al (2020) Towards a better understanding of the phase transformations in explosively welded copper to titanium sheets. Materials Science and Engineering: A 784. https://doi.org/10.1016/j.msea.2020.139285

54. Paul H, Skuza W, Chulist R et al (2020) The effect of interface morphology on the electro-mechanical properties of Ti/Cu clad composites produced by explosive welding. Metall Mater Trans A Phys Metall Mater Sci 51:750–766. https://doi.org/10.1007/s11661-019-05537-x

55. Greenberg BA, Ivanov MA, Pushkin MS et al (2016) Formation of intermetallic compounds during explosive welding. Metall Mater Trans A Phys Metall Mater Sci 47:5461–5473. https://doi.org/10.1007/s11661-016-3729-7

56. Zu G, Li X, Zhang J, Zhang H (2015) Interfacial characterization and mechanical property of Ti/Cu clad sheet produced by explosive welding and annealing. J Wuhan Univ Technol, Mater Sci Ed 30:1198–1203. https://doi.org/10.1007/s11595-015-1295-2

57. Yang M, Xu J, Ma H et al (2021) Microstructure development during explosive welding of metal foil: morphologies, mechanical behaviors and mechanisms. Compos B Eng 212:108685. https://doi.org/10.1016/j.compositesb.2021.108685

58. Yang M, Ma H, Shen Z, Sun Y (2019) Study on explosive welding for manufacturing meshing bonding interface of CuCrZr to 316L stainless steel. Fusion Eng Des 143:106–114. https://doi.org/10.1016/j.fusengdes.2019.03.137

59. Paul H, Chulist R, Lityńska-Dobrzyńska L, et al (2021) Interfacial reactions and microstructure related properties of explosively welded tantalum and steel sheets with copper interlayer. Mater Des 208. https://doi.org/10.1016/j.matdes.2021.109873

60. Najafi S, Khanzadeh MR, Bakhtiari H et al (2020) Electrochemical investigation of dissimilar joint of pure Cu to AISI 410 martensitic stainless steel fabricated by explosive welding. Surf Eng Appl Electrochem 56:675–683. https://doi.org/10.3103/S1068375520060113

61. Carvalho GHSFL, Galvão I, Mendes R et al (2023) The role of physical properties in explosive welding of copper to stainless steel. Def Technol 22:88–98. https://doi.org/10.1016/j.dt.2022.08.016

62. Xu JF, Ma HH, Shen ZW, Li YH (2022) Effects of interlayer on the interfacial microstructures and thermomechanical kinetics of explosive welded 2A14 aluminum alloy-niobium composite. Mater Today Commun 33:104792. https://doi.org/10.1016/j.mtcomm.2022.104792

63. Xu J, Ma H, Yang M et al (2022) Experimental and numerical investigations on the microstructural features and mechanical properties of explosive welded niobium-steel interface. Mater Des 218:110716. https://doi.org/10.1016/j.matdes.2022.110716

64. Prażmowski M, Rozumek D, Paul H (2017) Static and fatigue tests of bimetal Zr-steel made by explosive welding. Eng Fail Anal 75:71–81. https://doi.org/10.1016/j.engfailanal.2016.12.022

65. Baoxiang R, Gang T, Peng W, Changxing D (2019) Study on weldability window and interface morphology of steel tube and tungsten alloy rod welded by explosive welding. Int J Refract Metals Hard Mater 84:105005. https://doi.org/10.1016/j.ijrmhm.2019.105005

66. Zhao H, Sheng L (2021) Microstructure and mechanical properties of the Ag/316L composite plate fabricated by explosive welding. J Manuf Process 64:265–275. https://doi.org/10.1016/j.jmapro.2021.01.026

67. Narayan S, Tanaka S, Mori A, Hokamoto K (2017) Welding of Sn and Cu plates using controlled underwater shock wave. J Mater Process Technol 245:300–308. https://doi.org/10.1016/j.jmatprotec.2017.02.030